Dealing With Clouds and Seasonal Changes for Center Pivot Irrigation Systems Detection Using Instance Segmentation in Sentinel-2 Time Series

Anesmar Olino de Albuquerque, *Member, IEEE*, Osmar Luiz Ferreira de Carvalho, *Member, IEEE*, Cristiano Rosa e Silva, Argélica Saiaka Luiz, Pablo P. de Bem, *Member, IEEE*, Roberto Arnaldo Trancoso Gomes, *Member, IEEE*, Renato Fontes Guimarães, *Member, IEEE*, and Osmar Abílio de Carvalho Júnior, *Member, IEEE*

Abstract—The automatic detection of Center Pivot Irrigation Systems (CPIS) is fundamental for establishing public policies, especially in countries with a growth perspective in this technology, like Brazil. Previous studies to detect CPIS using deep learning used single-date optical images, containing limitations due to seasonal changes and cloud cover. Therefore, this research aimed to detect CPIS using Sentinel-2 multitemporal images (containing six dates) and instance segmentation, considering seasonal variations and different proportions of cloudy images, generalizing the models to detect CPIS in diverse situations. We used a novel augmentation strategy, in which, for each iteration, six images were randomly selected from the time series (from a total of 11 dates) in random order. We evaluated the Mask-RCNN model with the ResNext-101 backbone considering the COCO metrics on six testing sets with different ratios of cloudless ($< 20\%$) and cloudy images ($> 75\%$), from six cloudless images and zero cloudy images (6:0) up to one cloudless image and five cloudy images (1:5). We found that using six cloudless images provided the best metrics [80% average precision (AP), 93% AP with a 0.5 intersection over union threshold (AP50)]. However, results were similar (74% AP, 88% AP50) even in extreme scenarios with abundant cloud presence (1:5 ratio). Our method provides a more adaptive and automatic way to map CPIS from time series, significantly reducing interference such as cloud cover, atmospheric effects, shadow, missing data, and lack of contrast with the surrounding vegetation.

Index Terms—Cloud, deep learning, mask R-CNN, time series.

Anesmar Olino de Albuquerque, Cristiano Rosa e Silva, Argélica Saiaka Luiz, Pablo P. de Bem, Roberto Arnaldo Trancoso Gomes, Renato Fontes Guimarães, and Osmar Abílio de Carvalho Júnior are with the Department of Geography, University of Brasilia, Brasilia 70910-900, Brazil (e-mail: anesmar@ieee.org; cristiano@dubbox.com.br; argelica.saiaka@aluno.unb.br; pablodebem@gmail.com; robertogomes@unb.br; renatofg@unb.br; osmarjr@unb.br).

Osmar Luiz Ferreira de Carvalho is with the Department of Computer Science, University of Brasilia, Brasilia 70910-900, Brazil (e-mail: osmarcarvalho@ieee.org).

I. INTRODUCTION

STRATEGIES for technological advances in agricultural production are essential to feed the world's growing population [1], [2]. The technology-driven intensification with the increase in yield (production/area) is a viable solution to guarantee world food security and avoid expanding agricultural regions over natural environments [3]–[5]. Among the intensification procedures, irrigation plays a fundamental role in increasing agricultural productivity and decreasing costs and manual labor, being essential for crops in arid and semi-arid regions. Despite the benefits of irrigation for agriculture, it also negatively affects soil and water resources, such as reducing surface water and groundwater sources [6], [7], soil salinization [8], [9] erosion [10], [11], and ecological damage [12]. Besides, conflicts over water use increase, requiring governmental agencies to balance the diverse demands from hydroelectric production, irrigation, domestic, and industrial use. In the context of fast-growing water demand in the agriculture, constant irrigated area monitoring is crucial to predict and minimize current and potential conflicts. The main alternative for assessing the spatial distribution and estimating irrigated areas is the remote sensing monitoring because of its speed, periodicity, cost-effectiveness, and reliable data acquisition. Therefore, consistent remote sensing information on irrigation areas contributes to water management, anticipating necessary changes and negative impacts.

Among the various irrigation systems, the Center Pivot Irrigation System (CPIS) is one of the most advanced techniques consisting of water sprinklers in a suspended structure along a radius that rotates throughout the circular area, ensuring a uniform water distribution in the crops. The main advantages of the CPIS are efficient water and energy consumption, less workforce, easy operation, long-distance irrigation, and application of different types of fertilizers.

CPIS is the predominant irrigation technology in Central Brazil (Cerrado biome) due to the favorable environmental conditions with extensive flat topography and surface and underground water availability. The Cerrado biome has approximately 80% of all Brazilian CPIS [13]. However, the growing number of CPIS has led to intensified conflicts over water use and the need for governance of water resources [14]. In this context, the
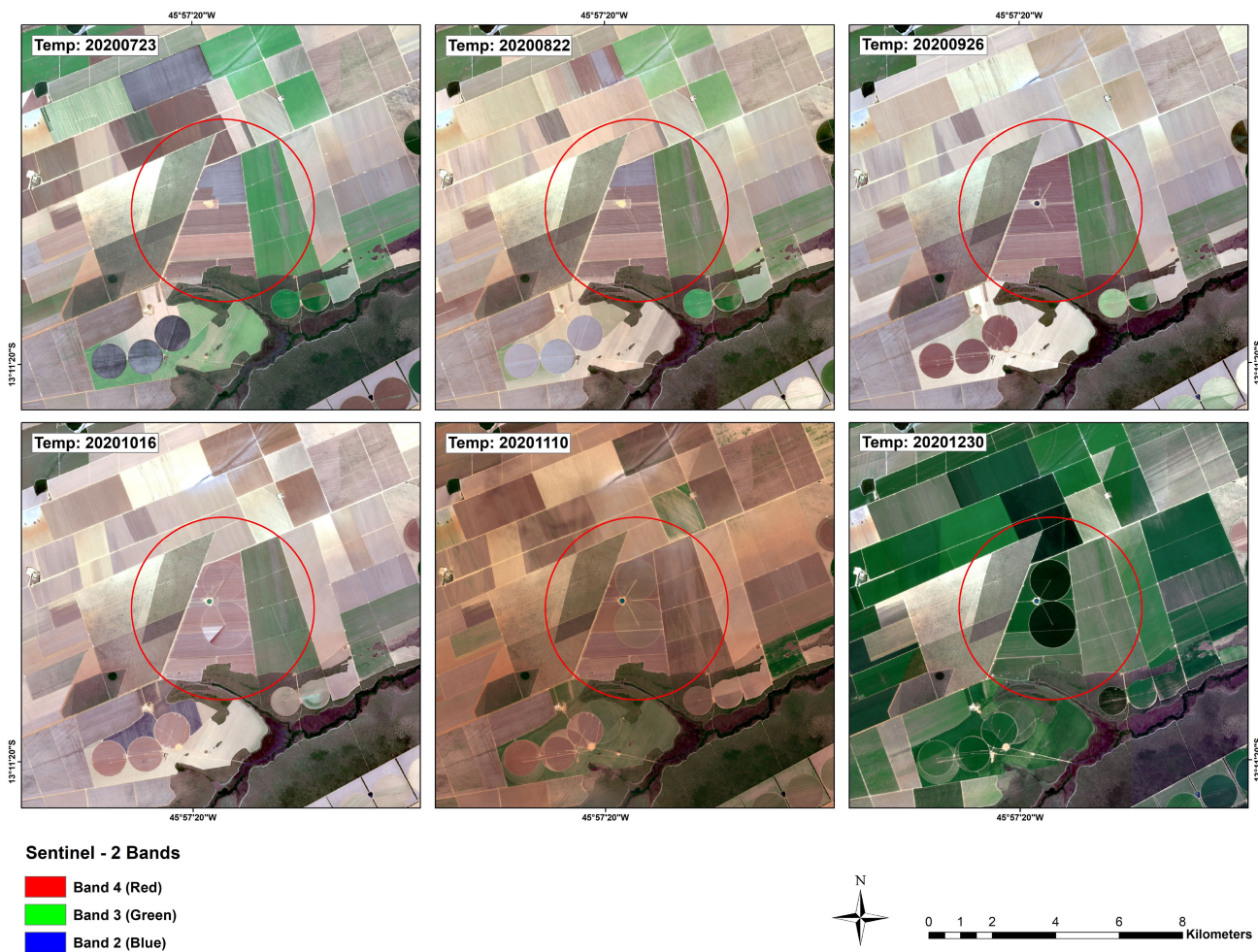
Fig. 1.   Representation of the seasonal variations among center pivots in a Sentinel-2 image using the Red, Green, and Blue spectral bands.

National Water Agency (ANA—*Agência Nacional de Águas*) performs the annual CPIS mapping based on remote sensing and visual interpretation images [15], [16]. In the quest to automate CPIS detection, methods based on deep learning (DL) have achieved results with metrics over 90% [17]–[20]. This approach allows for several advantages such as lower costs, faster, and more accurate surveying when compared to visual interpretation and traditional machine learning methods.

DL acts in solving problems in different areas of knowledge, including image, video, speech, and audio recognition [21]. Besides, DL models offers the opportunity to automate systems with high performance in processing large data sets by using computers with high storage and processing capacity and GPUs. Therefore, DL has promoted notable advances recently in the field of computer vision, allowing a high learning power of complex, subtle, and abstract representations directly from the data [22]. DL's extraordinary progress has had significant repercussions for the remote sensing community, with an expressive increase in the number of papers after 2014 [23]. In a short period, different review articles focused on DL in remote sensing, considering the different applications [24]; digital image processing (image fusion, image registration, classification, change detection, object detection, and segmentation) [23], [25]–[29]; environmental processes (land cover, vegetation parameters, agricultural yield prediction, air temperature, aerosol, particulate matter, precipitation, soil moisture, snow cover, evapotranspiration, radiation parameters, and ocean color parameters) [30]; status and perspectives [31]; and types of images (hyperspectral, multispectral, SAR, PolSAR, high spatial resolution, multimodal data fusion, and 3-D reconstruction) [32]–[36].

Convolutional neural networks (CNNs)-based models lead remote sensing studies due to the impressive accuracy in object recognition [28]. The CNN application in remote sensing images is more complex than in traditional red, green, and blue images. It requires geospatial systems, labeled data considering the different sensors and high image dimensionality (spatial, spectral, and temporal), clipping frames in specific sizes for training and segmentation, and image reconstruction procedure through sliding windows with overlapping pixels [37], [38].

There are three main difficulties associated with the mapping of center pivots using the optical image and deep learning: 1) seasonal planting variation that eventually merges with the surrounding areas (see Fig. 1); 2) cloud cover that prevents the detection of the Earth's surface; and 3) large-scale automated

processing. The previous studies for CPIS detection using DL on optical images considered a single time frame, requiring a specialist to identify the best dates in which the CPIS are more visible, and depending on the dates, the accuracy metrics may vary due to the seasonal changes which makes the CPIS very similar to their surroundings [18].

The present research aims to develop a procedure to annually inventory the center pivots using Sentinel-2 multitemporal images and a distinct semantic identification for each CPIS, seeking to circumvent ambiguities due to the interannual variability in the crop stage and the presence of cloud cover or shadows. To this end, we developed a multitemporal database considering different planting stages and with different proportions of cloud cover. The control of the cloud-cover proportion used an algorithm that randomly introduced images with a high percentage of cloud cover in the time series. Therefore, the methodology assesses the learning ability of CNN architectures to detect targets without having complete information over time. Besides, the CNN model combined spatial-temporal spectral information.

II. RELATED WORKS

The governmental interest in CPIS's water and energy consumption and agricultural production caused an increase in remote sensing studies for their detection. Although the circular shape of the center pivot is very characteristic, its automatic detection has limitations for traditional image classification methods [39]. The CPIS do not have uniform spatial and temporal behavior internally, containing different plantings (with subdivision of the area or intercropped) and diversity for the surrounding CPIS (with different agricultural crops and crop production cycles) [18]. These peculiarities make the pixel-based classifications considering the spectral response, vegetation indices, or temporal signatures very deficient. The inclusion of spatial attributes to consider center-pivot shape presents a challenge for remote sensing studies that have only recently been overcome. Therefore, different approaches to center pivot mapping by remote sensing have been used, such as a) visual interpretation, b) Hough transform, c) Geographic object-based image analysis (GEOBIA), and d) DL methods.

The first studies of CPIS mapping in the 70s and 80s used the visual interpretation of circular features [40], [41], which is still a widely used method [42]–[45]. Despite the precise results with a visual interpretation, the process is laborious and time-consuming.

Although the Hough Transform (HT) is a technique for automatically detecting circles, with a promising perspective for detecting center pivots, few studies are on its application [19], [46]. The main limitations of the HT method are complex parameter setting, low precision, long computational time, and difficulty in situations with incomplete circles [20], [47].

GEOBIA combines segmentation methods which partition images into objects and a set of rules that allow intuitive step-by-step classification. This object-based approach can have advantages over pixel-based approaches, incorporating spatial attributes derived from the object's shape, hierarchical multiscale information, texture, and class-related characteristics [48]–[50].

The GEOBIA studies for detecting CPIS consider variations in the methodological sequence and attributes used [51]–[53]. Yan and Roy [52] established three stages in the mapping of center pivots using GEOBIA: a) object-based approach (active geometric contour based on the variational region); b) segmentation method (watershed algorithm); and c) geometry-based algorithm to detect rectangular, circular, and irregularly shaped fields. Johansen *et al.* [51] describe four steps in center pivot detection: a) generation of the annual maximum image of the Normalized Difference Vegetation Index and the annual panchromatic band, b) segmentation, c) classification using the shape such as the center pivot field length, length–width ratio, and elliptical adjustment, and d) the rule-set definition.

However, several studies demonstrate an overall superiority of DL to GEOBIA regarding different factors: a) greater precision and efficiency; b) less human supervision; c) reuse of knowledge due to the high capacity for transferability to other regions or scenarios considering the various attributes of the object (light, color, background, size, and shape); and d) less interference by salt and pepper noise [54]–[56].

Recently, the CPIS has been a constant target for DL studies using CNNs with different approaches: a) detection of the core point of the center pivot [47]; b) object detection with the establishment of bounding boxes around CPIS [20], [57]; c) semantic segmentation that performs a pixel-wise classification where all CPIS pixels receive a label [18], [58], [59]; and d) instance segmentation that produces bounding boxes and pixel-wise segmentation masks on CPIS [17].

Among the CNNs-based models applied in CPIS, the instance segmentation approach is the most complex and advantageous. It allows extracting individual instance for each CPIS in an image and acquiring more information such as the total number of CPIS and area per unit. Besides, instance segmentation has a greater ability to separate overlapping objects of the same class. The most used instance segmentation methods are FCIS [60] and Mask-RCNN [61], which first perform the instance step and then perform the segmentation and classification in parallel.

In contrast to the above methods for center pivot detection, the proposed method searches greater discrimination of the center pivot by incorporating the temporal data to overcome the influences of the images altered by the cloud cover or periods of similar behavior between the pivot and the surrounding area.

III. MATERIALS AND METHODS

We applied the following methodology: A) Study area; B) image acquisition; C) annotations; D) instance segmentation approach; and E) large image classification.

A. Study Area

The study areas are located in Central Brazil, containing the country's highest CPIS concentrations due to the flat terrain and water potential that allows mechanization and irrigation. The Central Brazil region is mostly used in studies with deep learning to CPIS detection (Table 1). The low rainfall between May and September prevents several crops, which becomes viable with irrigation. This research considered two main CPIS
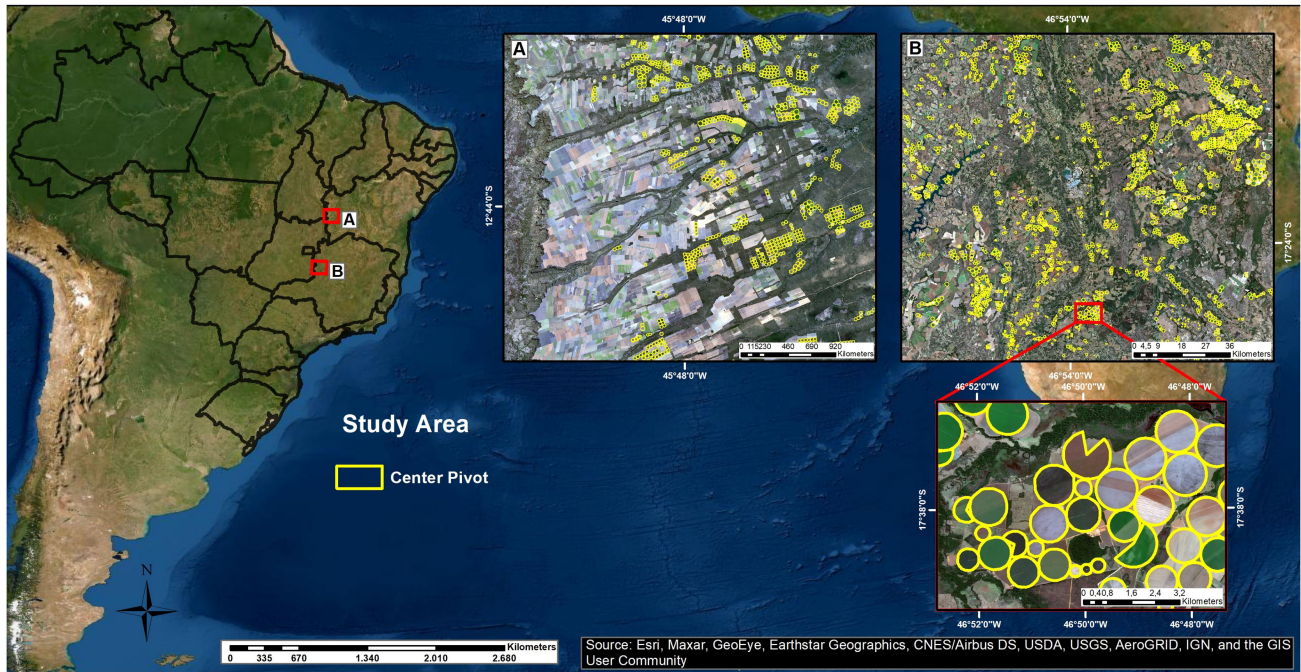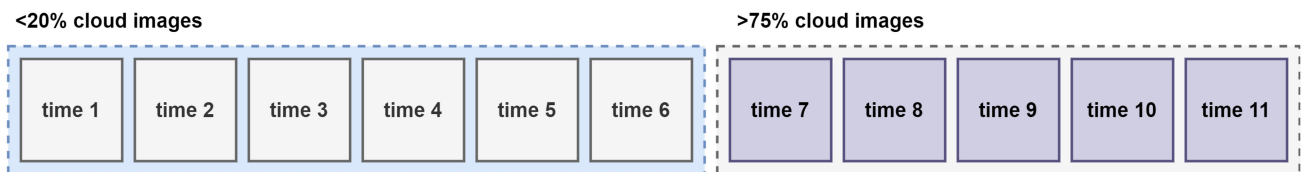
Fig. 2.   Study area.

Fig. 3.   Representation of the constructed time series, in which the first six temporal frames (temp) are images with less than 20% of cloud cover and from temp 7 to temp 11, the images contain more than 75% of cloud cover.

concentrations within Central Brazil: a) Western Bahia and b) region between the states of Minas Gerais and Goiás close to the Federal District (see Fig. 2). Western Bahia presents a significant growth in mechanized agriculture [63], [64] and an intensification of center pivots, ranging from 9 in 1985 to 1550 in 2016 [65]. The Goiás/Minas Gerais region contains hundreds of CPIS, resulting in an intensification of the water-use conflicts due to the competition between irrigation, human consumption, and hydroelectric power generation [14].

B. Image Acquisition and Time Series Construction

The Sentinel-2 mission developed by the European Space Agency (ESA) under the European Union's Copernicus program acquires high spatial resolution multispectral optical images [66]. This research uses images with 10-m spatial resolution corresponding to the spectral bands at 490, 560, 665, and 842 nm. The images acquired in Level 1 C have radiometric processing and geometric correction. In the Sentinel Application Platform (SNAP) software developed by ESA, we carry out the preprocessing steps.

In order to assess the seasonal and cloud interference, the elaboration of the time series encompassed 11 different dates, considering the dry and rainy periods and different percentages

of cloud images. We predetermined the percentage of cloud coverage in the time series, selecting and combining two image time series (cloudless and total cloud coverage). Therefore, we chose 11 temporal frames for each region, in which six times the criteria were less than 20% clouds and five times the criteria were more than 75% clouds (see Fig. 3). In addition, each temporal image contained four spectral bands (red, green, blue, and near-infrared). Thus, the final stacked image for each region presented a shape with $512(\text{height}) \times 512(\text{width}) \times 44(\text{bands})$.

C. Annotations and Split

Since the main objective of this research is to identify CPIS throughout a specified period, the ground truth elaboration carefully analyzed each temporal frame within the time series. If a CPIS appeared at least once in any of the temporal frames, we annotated it using the ArcGIS software. The basis for the annotations was the vector data of the ANA, duly corrected considering the visual interpretation. However, Detectron2's Mask-RCNN algorithm requires labels in the COCO annotation format [67], in which each image tile needs a JSON file with the corresponding annotations. Thus, we applied the method used by de Carvalho et al. [17] to convert polygonal GIS data into the instance segmentation annotation format. Each object acquired

TABLE I
PREVIOUS STUDIES ON CENTER PIVOT IRRIGATION SYSTEMS DETECTION, AND THEIR CORRESPONDING REGION, SATELLITE, METHOD, MODEL, AND BANDS

Paper	Region	Satellite	Method	Model	Bands
[47]	Colorado, USA	TM-Landsat 5	Central point detection	LeNet-5, AlexNet, VGGNet	RGB
[58]	Central Brazil Texas, USA	PlanetScope	Semantic	U-Net	RGB-NIR
[59]	Duero, Spain South Africa	Sentinel-2	Semantic	U-Net	4 bands/ 3 PCAs
[19]	Central Brazil	Sentinel-2	object detection	PVANET-Hough	RGB
[20]	Central Brazil	Sentinel-2	object detection	PVANET, YOLOv4	RBG+filters
[18]	Central Brazil	Landsat-8	semantic	U-net, Deep ResUnet, SharpMask	7 bands
[17]	Central Brazil	Landsat-8	instance	Mask-RCNN (7 backbone structures)	RGB/7 bands
[62]	Central Brazil	Sentinel-1	instance	Mask-RCNN	Multitemporal (10 times)

TABLE II
NUMBER OF IMAGES AND INSTANCES WITHIN THE TRAINING (TRAIN),
VALIDATION (VAL), AND TESTING (TEST) SETS

Set	# of images	# of instances
Train	1000	7071
Val 1, 2, 3, 4, 5, and 6	300	2480
Test 1, 2, 3, 4, 5, and 6	300	2480

a unique value from 1 to *N*, with *N* being the total number of CPIS.

The software automatically generates a folder with the cropped images and the annotations for each image in the COCO annotation format. We distribute the image tiles in training, validation, and test sets, considering MG/GO area (2018 and 2020) as training data, Western Bahia area of 2020 for validation, and 2018 for testing. We selected 500 points for each MG/GO area image for training, totaling 1000 images. Table II shows the distribution regarding the number of images and the number of instances in each set.

1) Training Images: From each MG/GO region image (2018 and 2020), we selected 500 training samples (totaling 1000 samples). Even though the temporal series presents 11 dates, the input model considered only six dates. In the training procedure, we used a novel augmentation technique that selects six temporal events (from the 11 total bands) in a shuffled order, corresponding to an image with the following dimensions: 512 (width) × 512 (height) × 24 (spectral-temporal bands). The selection among six cloudless images and five cloudy images ensured that the training sample had at least one cloudless event, preventing the algorithm from having only cloudy events, which would yield only errors. Furthermore, random selection helps avoid overfitting, and in a practical application, there is no concern with the order of images.

2) Validation and Test Images: The test stage used the image of Western Bahia 2018, and the validation stage used Western Bahia 2020. Unlike the training examples in which the order of the images does the shuffling in each iteration, the test and validation examples consider combinations with different percentages of cloud events to assess their influence. Thus, we evaluated the trained model in six configurations with the following cloudless:cloud ratios: 1) 6:0; 2) 5:1; 3) 4:2; 4) 3:3; 5) 2:4; and 6) 1:5. Furthermore, we made five random combinations

for each selected sampling area to increase the number of the samples and avoid possible bias. In this sense, the selection of the test and validation samples considered 60 areas, resulting in 300 samples with a different ordering.

D. Instance Segmentation Approach

Among the instance segmentation models, the Mask-RCNN is the most common approach. The Mask-RCNN algorithm has three objectives: a) identify the bounding box for a given object, b) classify that bounding box according to the object's class, and c) perform pixel-wise binary segmentation mask on the object. For this reason, the total loss function is given by the sum of the bounding box loss ($Loss_{\text{bbox}}$), mask loss ($Loss_{\text{mask}}$), and classification loss ($Loss_{\text{class}}$): $Loss_{\text{total}} = Loss_{\text{mask}} + Loss_{\text{class}} + Loss_{\text{bbox}}$, where $Loss_{\text{mask}}$ and $Loss_{\text{class}}$ are the log loss function, and $Loss_{\text{bbox}}$ is the L1 loss.

Detectron2 [68] is one of the most efficient instance segmentation frameworks, introduced by the Facebook Artificial Intelligence Research (FAIR), powered by Pytorch. This architecture, usually applied to traditional RGB imagery, requires adjustments to be compatible with the remote sensing data [17]. Hence, we use the Detectron2 software from the Pytorch library with some adaptations to suit our purposes. The software uses some standard settings for traditional DL datasets, such as COCO and Cityscapes. However, for remote sensing images, some changes are necessary for a better adjustment of the models. We need to change the number of input channels on the network (since the most common approach uses only RGB channels). Consequently, the input network increased to 24 channels since the analysis used six temporal events, in which each event contains four channels (red, green, blue, and near-infrared).

1) Model Configurations: To train the Mask-RCNN model, we made the necessary source code changes for compatibility reasons. Since one of our main objectives was to evaluate cloud occlusion, all experiments considered the same backbone structure, the ResNeXt-101-32x8d (X-101) [69]. As augmentation strategies to avoid overfitting, we applied the random choice of temporal images for each iteration, random horizontal flip, and random vertical flip. Furthermore, this procedure broke the dependence of temporal structures, i.e., the order of images in the temporal structure becomes irrelevant.

Regarding hyperparameters, we applied a) Adam optimizer with a learning rate of 0.0005; b) 256 Region of Interest (ROIs)

TABLE III
RESULTS FOR THE BOUNDING BOX AND MASK PREDICTIONS ON THE DIFFERENT TEST SETS WITH DIFFERENT RATIOS OF CLOUDLESS AND CLOUDY IMAGES IN THE TIME SERIES

Ratio (cloudless:cloudy)	Box						Mask					
	AP	AP50	AP75	APs	APm	APl	AP	AP50	AP75	APs	APm	APl
6:0	80.10	93.71	91.09	18.43	78.39	86.20	80.21	93.75	90.58	16.91	78.21	86.98
5:1	79.83	92.97	91.08	17.86	78.45	86.06	79.98	93.85	90.56	16.68	78.31	86.59
4:2	79.50	92.83	90.75	17.77	77.95	85.90	79.53	92.94	89.76	16.60	77.63	86.37
3:3	79.12	92.14	90.10	18.51	76.41	85.91	79.20	92.17	89.73	17.43	76.21	86.29
2:4	77.85	91.13	88.14	17.23	75.32	84.45	78.04	91.04	88.05	16.68	74.55	85.24
1:5	74.17	88.26	85.36	14.66	70.57	81.78	74.89	88.20	85.31	14.41	70.17	82.69

per image; c) 30 000 iterations; and anchor boxes with 16, 32, 64, 128, 256. The other parameters were used as default. We used Nvidia GeForce RTX 2080 TI GPU with 11 GB memory to process and train the model.

E. Accuracy Analysis

The model evaluation considered the COCO metrics [67] average precision (AP), AP50, AP75, APs, APm, and APl. These metrics are the most widely used in instance segmentation problems and have proven to be satisfactory to evaluate different models, including the original Mask-RCNN paper [61] and other influential papers on the subject [70]–[73]. The AP is a ranking metric that considers the area under the precision–recall curve. However, the COCO AP also considers ten Intersection over Union thresholds (IoU) (from 0.5 to 0.95 with 0.05 steps). AP50 and AP75 scores consider a fixed threshold of 0.5 (more permissive) and 0.75 (stricter). Moreover, APsmall, APmedium, and APlarge consider the sizes of the different objects, in which small objects have areas of 32^2 or lower, medium objects have areas between 32^2 and 96^2, and large objects have areas larger than 96^2.

IV. RESULTS

A. Cloud Interference and Performance Metrics

Table III lists the detection (Box) and segmentation (Mask) results with different ratios of cloudless and cloudy images using the X-101 backbone. The main metric (AP) decreases with the increase of cloudy images proportion in the time series for both the bounding box and the mask predictions. The maximum difference between the AP values (6:0–1:5) is not expressive, reaching 5.93 for the bounding box and 5.32 for the mask prediction. Moreover, the box and mask results are similar, mainly because of the CPIS round shape, which yields similar IoU results for the boxes and segmentation masks. This result demonstrates the ability of the DL method to detect features even under conditions of little information (low presence of cloudless images) in the time series. The most extensive ranges of variation are between time series with the lowest cloudless image ratio (1:5 and 2:4). In contrast, time series containing high cloudless image rates maintain high values and are close to each other. This behavior is predictable, where the smaller proportion of cloudless images increases the seasonal effect and the probability of not obtaining adequate images to detect center pivots.

The other precision measures (AP50, AP75, APsmall, APmedium, and APlarge) tend to show the same general behavior of decreasing values with an increasing proportion of cloudless images. The only exception was the APm, which had a position inversion between the 6:0 and 5:1 ratios, despite the very close values. This experiment shows scenarios with a very extreme cloud image in the time series, still showing good results.

Among the metrics evaluated, APs had the worst results. The main factor for the poor performance of small objects is that they represent partial forms of CPIS positioned on the edges of the frame, which in the sample cut became incomplete and small. Therefore, the sample edges are more susceptible to detection errors, which can be minimized with the application of the moving window mosaic [17].

Fig. 4 shows the prediction of the same region with different ratios of cloud presence in the time series. The result demonstrates that even in the most extreme scenarios, with five cloudy images and only one cloudless image, the instance segmentation obtained correct predictions. The modifications identified between the different predictions concentrated on minor variations in the center pivot design. Besides, there are inaccuracies in detecting a small part of a center pivot cut in the left corner of the third alignment of the CPISs. As the proportion of clouds increases, the small slice of a center pivot disappears.

B. Seasonal Interference

Eventually, the CPIS patterns fade with the surrounding areas, and the detection is not possible. The use of multitemporal images guarantees the acquisition of data in the different planting stages that evidence the presence of CPIS.

Fig. 5 presents nine examples containing instance segmentation results and the color compositions of the six temporal images used as input. The Sentinel-2 images correspond to images with a percentage of clouds below 25%. This condition would be a viable criterion to compose the six multitemporal images, allowing to obtain a vast predominance of free-cloud images, different phases of the planting cycle, and a viable set for automation with good precision. The temporal sequence demonstrates that some center pivots practically disappear in specific periods, becoming very similar to their surroundings,
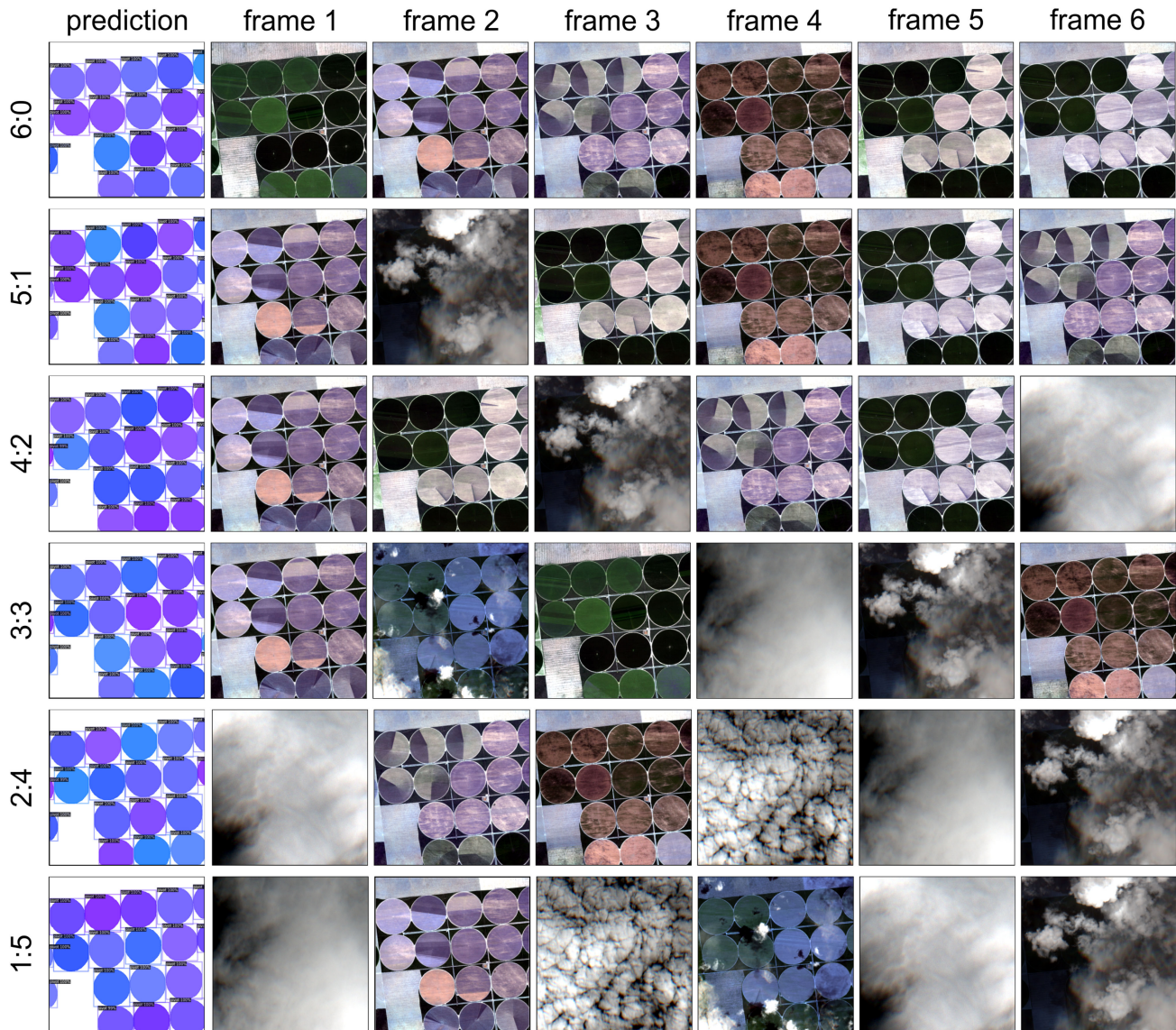
Fig. 4. Representation of the predictions of a given region using the different ratios of cloud presence, in which each bounding box with the segmentation mask represents a different instance of center pivots.

making their detection very difficult even by visual interpretation. A clear example is the images of row A, where some images (frames 1–2–3) are visible only in three center pivots, despite the existence of four CPIS as evidenced by the last image (frame 6). The other images present CPIS with behavior like the background in a certain period.

Therefore, the different behaviors of CPIS over time make it difficult to generalize a DL model to a single date. The model with multitemporal data allows high generalizability and a precise classification, even in cases where the CPIS becomes imperceptible or in the presence of clouds in a temporal interval.

V. DISCUSSION

All DL models applied to optical imaging for center pivot detection reported training and applications for single-time imaging [17], [18], [20], [47], [57]–[59]. The main problems from only one date are clouds and visualizing the center pivot in particular planting stages. De Albuquerque *et al.* [18] showed that there are periods of the year that are easier to identify CPIS due to seasonal changes. According to the authors, the end of the drought and rainy seasons in Central Brazil present more significant difficulties. The best period is the onset of drought when the natural environment has nonphotosynthetically active vegetation, and the irrigated pivots have photosynthetically active vegetation.

Therefore, a viable solution to overcome the problems described is developing DL models adapted to a set of temporal images. Recently, a study using Sentinel-1 radar images used DL models of time series to detect center pivots [62]. Although radar data is free from cloud interference, research has shown that increasing the number of images has improved instance segmentation accuracy.
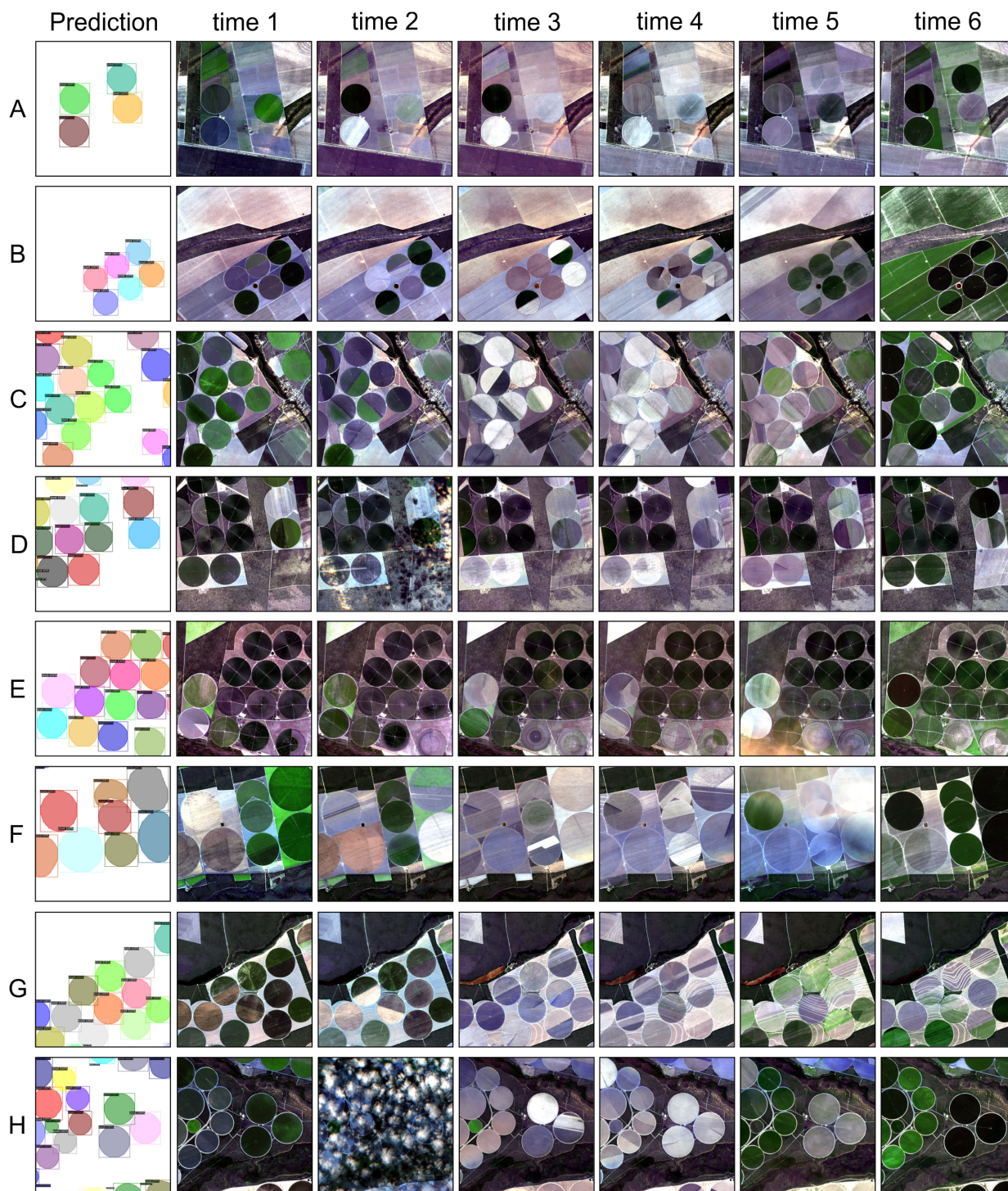
Fig. 5.　Representation of nine predictions and their respective cloudless ($< 20\%$ cloud cover) time series. Note that even with this percentage, there is still a chance of having cloudy frames, as shown in F and H.

This multitemporal approach with DL algorithms allows a more generalized learning that captures the uniform shape of the center pivot, disregarding the images with the presence of clouds and variations in the plantations. Furthermore, the model presents efficiency independent of the temporal order of the images. This approach of looking for an invariant shape over a period differs from studies that distinguish the types of crops that depend on the phenological cycle, and the chronological

sequence [74], [75]. In this context, we developed a new strategy to increase the number of samples and reduce the chances of overfitting, randomly selecting the order of images in the time series. Training and evaluation considered different cloud proportions and the image ordering allows for a greater flexibility in data acquisition and automation.

The proposed methodology represents a robust alternative to the CPIS surveys carried out by the Brazilian government

based on the visual interpretation of images [15], [16]. The procedure has significant advantages in terms of speed and consideration of multitemporal images, not limited to a specific date. Furthermore, the present DL approach with multitemporal optical images can be effectively applied to other objects with a fixed format within a time interval of interest, such as buildings and solar panels.

VI. Conclusion

The present study proposed a new DL approach for CPIS detection using time series, including different cloud occlusion scenarios and seasonal behavior, problems of great interest in the study of optical images. Unlike single-date data, multitemporal data offers more opportunities to observe center pivots by overcoming optical imaging issues such as cloud cover, atmospheric effects, shadow, missing data, and lack of contrast to surrounding vegetation. In addition, time-series satellite images reduce ambiguities arising from the phenological stage and the spatial boundary of the CPIS.

We proposed a new augmentation strategy for time series analysis in which we randomly select images from the time series, introducing different percentages of cloudy images. The procedure forces the neural network to learn with the presence of images containing atmospheric interference and spectral similarity between the center pivot and the surrounding areas. However, this procedure only applies to objects that present similar structures over time, as is the case with CPIS.

Predictably, we found that results were better when using a time series with images with a low cloud presence. Nonetheless, results kept steady even in more extreme scenarios, demonstrating a good generalization capability. Furthermore, this approach to targets with spectral variation over time within a fixed shape favors the generalization of the model, as it captures different scenarios of the same object and increases the predictive power. The results show an excellent perspective for practical application, obtaining good results from six images without a rigorous selection for better detection. The algorithm returns a very precise classification result. This model favors automation of CPIS detection with cost savings and agility, and and avoids large consumption of labor.

References

[1] H. C. J. Godfray *et al.*, "Food security: The challenge of feeding 9 billion people," *Science*, vol. 327, no. 5967, pp. 812–818, 2010.

[2] A. Y. Prosekov and S. A. Ivanova, "Food security: The challenge of the present," *Geoforum*, vol. 91, pp. 73–77, 2018.

[3] A. Beltran-Peña, L. Rosa, and P. D'Odorico, "Global food self-sufficiency in the 21st century under sustainable intensification of agriculture," *Environ. Res. Lett.*, vol. 15, no. 9, 2020, Art. no. 095004.

[4] J. A. Foley *et al.*, "Solutions for a cultivated planet," *Nature*, vol. 478, no. 7369, pp. 337–342, 2011.

[5] P. M. Kopittke, N. W. Menzies, P. Wang, B. A. McKenna, and E. Lombi, "Soil and the intensification of agriculture for global food security," *Environ. Int.*, vol. 132, 2019, Art. no. 105078.

[6] Y. Guang, H. Xinlin, L. Xiaolong, L. Aihua, and X. Lianqing, "Transformation of surface water and groundwater and water balance in the agricultural irrigation area of the Manas river basin, China," *Int. J. Agricultural Biol. Eng.*, vol. 10, no. 4, pp. 107–118, 2017.

[7] H. I. Essaid and R. R. Caldwell, "Evaluating the impact of irrigation on surface water-groundwater interaction and stream temperature in an agricultural watershed," *Sci. Total Environ.*, vol. 599, pp. 581–596, 2017.

[8] Z. Wang, B. Fan, and L. Guo, "Soil salinization after long-term mulched drip irrigation poses a potential risk to agricultural sustainability," *Eur. J. Soil Sci.*, vol. 70, no. 1, pp. 20–24, 2019.

[9] A. Tomaz *et al.*, "Risk assessment of irrigation-related soil salinization and solidification in Mediterranean areas," *Water*, vol. 12, no. 12, 2020, Art. no. 3569.

[10] R. Sojka, "Understanding and managing irrigation-induced erosion," in *Advances in Soil and Water Conservation*. Boca Raton, FL, USA: CRC Press, 2018, pp. 21–37.

[11] M. Abu-Hashim, A. Sayed, M. Zelenakova, Z. Vranayová, and M. Khalil, "Soil water erosion vulnerability and suitability under different irrigation systems using parametric approach and Gis, Ismailia, Egypt," *Sustainability*, vol. 13, no. 3, 2021, Art. no. 1057.

[12] Q. Zhang, Z. Zhang, P. Shi, V. P. Singh, and X. Gu, "Evaluation of ecological instream flow considering hydrological alterations in the Yellow river basin, China," *Glob. Planet. Change*, vol. 160, pp. 61–74, 2018.

[13] D. Althoff and L. N. Rodrigues, "The expansion of center-pivot irrigation in the Cerrado biome," *Irrigate*, vol. 1, no. 1, pp. 56–61, 2019.

[14] L. M. daCosta Silva *et al.*, "Conflito pelo uso da água na bacia hidrográfica do rio são marcos: O estudo de caso da uhe batalha," *Engevista*, vol. 17, no. 2, pp. 166–174, 2015.

[15] Agência Nacional de Águas, *Levantamento da Agricultura Irrigada por Pivôs Centrais no Brasil - 2014: Relatório Síntese*, Agência Nacional de Águas (ANA), ed., Brasília, Brasil: Agência Nacional de Águas (ANA), 2016.

[16] Agência Nacional de Águas, *Levantamento da agricultura irrigada por pivôs centrais no Brasi (1985–2017)*. Brasília, Brasil: *Agência Nacional de Águas (ANA)*, Embrapa Milho e Sorgo, 2019. [Online]. Available: https://www.ana.gov.br/noticias/ana-e-embrapa-identificam-forte-tendencia-de-crescimento-da-agricultura-irrigada-por-pivos-cent rais-no-brasil/ana_levantamento-da-agricultura-irrigada-por-pivos-cent rais_2019.pdf (accessed on 1 June 2019).

[17] O. L. F. d. Carvalho *et al.*, "Instance segmentation for large, multi-channel remote sensing imagery using mask-RCNN and a mosaicking approach," *Remote Sens.*, vol. 13, no. 1, 2021, Art. no. 39.

[18] A. O. de Albuquerque *et al.*, "Deep semantic segmentation of center pivot irrigation systems from remotely sensed data," *Remote Sens.*, vol. 12, no. 13, 2020, Art. no. 2159.

[19] J. Tang, D. Arvor, T. Corpetti, and P. Tang, "Pvanet-Hough: Detection and location of center pivot irrigation systems from Sentinel-2 images," *ISPRS Ann. Photogrammetry, Remote Sens. Spatial Inf. Sci.*, vol. 3, pp. 559–564, 2020.

[20] J. Tang, Z. Zhang, L. Zhao, and P. Tang, "Increasing shape bias to improve the precision of center pivot irrigation system detection," *Remote Sens.*, vol. 13, no. 4, 2021, Art. no. 612.

[21] W. Liu, Z. Wang, X. Liu, N. Zeng, Y. Liu, and F. E. Alsaadi, "A survey of deep neural network architectures and their applications," *Neurocomputing*, vol. 234, pp. 11–26, 2017.

[22] L. Liu *et al.*, "Deep learning for generic object detection: A survey," *Int. J. Comput. Vis.*, vol. 128, no. 2, pp. 261–318, 2020.

[23] G. Cheng, X. Xie, J. Han, L. Guo, and G.-S. Xia, "Remote Sensing Image Scene Classification Meets Deep Learning: Challenges, Methods, Benchmarks, and Opportunities," *IEEE J. Sel. Topics Appl. Earth Observ. Remote Sens.*, vol. 13, pp. 3735–3756, 2020.

[24] J. E. Ball, D. T. Anderson, and C. S. Chan Sr., "Comprehensive survey of deep learning in remote sensing: Theories, tools, and challenges for the community," *J. Appl. Remote Sens.*, vol. 11, no. 4, 2017, Art. no. 042609.

[25] T. Hoeser, F. Bachofer, and C. Kuenzer, "Object detection and image segmentation with deep learning on Earth observation data: A review-Part II: Applications," *Remote Sens.*, vol. 12, no. 18, 2020, Art. no. 3053.

[26] L. Khelifi and M. Mignotte, "Deep learning for change detection in remote sensing images: Comprehensive review and meta-analysis," *IEEE Access*, vol. 8, pp. 126385–126400, 2020.

[27] Y. Li, H. Zhang, X. Xue, Y. Jiang, and Q. Shen, "Deep learning for remote sensing image classification: A survey," *Wiley Interdiscipl. Rev.: Data Mining Knowl. Discov.*, vol. 8, no. 6, 2018, Art. no. e1264.

[28] L. Ma, Y. Liu, X. Zhang, Y. Ye, G. Yin, and B. A. Johnson, "Deep learning in remote sensing applications: A meta-analysis and review," *ISPRS J. Photogrammetry Remote Sens.*, vol. 152, pp. 166–177, 2019.

[29] L. Zhang, L. Zhang, and B. Du, "Deep learning for remote sensing data: A technical tutorial on the state of the art," *IEEE Geosci. Remote Sens. Mag.*, vol. 4, no. 2, pp. 22–40, Jun. 2016.

[30] Q. Yuan *et al.*, "Deep learning in environmental remote sensing: Achievements and challenges," *Remote Sens. Environ.*, vol. 241, 2020, Art. no. 111716.

[31] J. Li, X. Huang, and J. Gong, "Deep neural network for remote-sensing image interpretation: Status and perspectives," *Nat. Sci. Rev.*, vol. 6, no. 6, pp. 1082–1086, 2019.

[32] M. Paoletti, J. Haut, J. Plaza, and A. Plaza, "Deep learning classifiers for hyperspectral imaging: A review," *ISPRS J. Photogrammetry Remote Sens.*, vol. 158, pp. 279–317, 2019.

[33] H. Parikh, S. Patel, and V. Patel, "Classification of SAR and polsar images using deep learning: A review," *Int. J. Image Data Fusion*, vol. 11, no. 1, pp. 1–32, 2020.

[34] A. Signoroni, M. Savardi, A. Baronio, and S. Benini, "Deep learning meets hyperspectral image analysis: A multidisciplinary review," *J. Imag.*, vol. 5, no. 5, p. 52, 2019.

[35] A. Vali, S. Comai, and M. Matteucci, "Deep learning for land use and land cover classification based on hyperspectral and multispectral earth observation data: A review," *Remote Sens.*, vol. 12, no. 15, 2020, Art. no. 2495.

[36] X. X. Zhu *et al.*, "Deep learning in remote sensing: A comprehensive review and list of resources," *IEEE Geosci. Remote Sens. Mag.*, vol. 5, no. 4, pp. 8–36, Dec. 2017.

[37] P. P. de Bem, O. A. de Carvalho Júnior, O. L. F. de Carvalho, R. A. T. Gomes, and R. Fontes Guimarães, "Performance analysis of deep convolutional autoencoders with different patch sizes for change detection from burnt areas," *Remote Sens.*, vol. 12, no. 16, 2020, Art. no. 2576.

[38] Y. Yi, Z. Zhang, W. Zhang, C. Zhang, W. Li, and T. Zhao, "Semantic segmentation of urban buildings from VHR remote sensing imagery using a deep convolutional neural network," *Remote Sens.*, vol. 11, no. 15, 2019, Art. no. 1774.

[39] M. Ozdogan, Y. Yang, G. Allez, and C. Cervantes, "Remote sensing of irrigated agriculture: Opportunities and challenges," *Remote Sens.*, vol. 2, no. 9, pp. 2274–2304, 2010.

[40] R. C. Heller and K. A. Johnson, "Estimating irrigated land acreage from landsat imagery," *Photogrammetric Eng. Remote Sens.*, vol. 45, no. 10, pp. 1379–1386, 1979.

[41] M. P. Carlson, "The Nebraska center-pivot inventory: An example of operational satellite remote sensing on a long-term basis," *Photogrammetric Eng. Remote Sens.*, vol. 55, pp. 587–590, 1989.

[42] E. N. Demarqui and L. M. B. Demarqui, "Análise espaço-temporal da ocorrência de sistemas de irrigação por pivê central em regiões agrícolas no estado de mato grosso," *Nativa*, vol. 8, no. 3, pp. 344–351, 2020.

[43] E. Ferreira, J. H. d. Toledo, A. A. Dantas, and R. M. Pereira, "Cadastral maps of irrigated areas by center pivots in the state of Minas Gerais, using CBERS-2B/CCD satellite imaging," *Engenharia Agrícola*, vol. 31, no. 4, pp. 771–780, 2011.

[44] J. D. Martins, I. S. Bohrz, E. F. Tura, M. Fredrich, R. P. Veronez, and G. A. Kunz, "Levantamento da área irrigada por pivê central no estado do rio grande do sul," *IRRIGA*, vol. 21, no. 2, pp. 300–300, 2016.

[45] K. Wenger, J. M. Vadjunec, and T. Fagin, "Groundwater governance and the growth of center pivot irrigation in Cimarron County, OK and Union County, NM: Implications for community vulnerability to drought," *Water*, vol. 9, no. 1, 2017, Art. no. 39.

[46] M. Rodrigues, T. Körting, G. de Queiroz, C. Sales, and L. da Silva, "Detecting center pivots in Matopiba using Hough transform and web time series service," in *Proc. IEEE Latin Amer. GRSS ISPRS Remote Sens. Conf.*, 2020, pp. 189–194.

[47] C. Zhang, P. Yue, L. Di, and Z. Wu, "Automatic identification of center pivot irrigation systems from landsat images using convolutional neural networks," *Agriculture*, vol. 8, no. 10, p. 147, 2018.

[48] T. Blaschke, "Object based image analysis for remote sensing," *ISPRS J. Photogrammetry Remote Sens.*, vol. 65, no. 1, pp. 2–16, 2010.

[49] M. D. Hossain and D. Chen, "Segmentation for object-based image analysis (OBIA): A review of algorithms and challenges from remote

[50] S. Ye, R. G. Pontius Jr., and R. Rakshit, "A review of accuracy assessment for object-based image analysis: From per-pixel to per-polygon approaches," *ISPRS J. Photogrammetry Remote Sens.*, vol. 141, pp. 137–147, 2018.

[51] K. Johansen, O. Lopez, Y.-H. Tu, T. Li, and M. F. McCabe, "Center pivot field delineation and mapping: A satellite-driven object-based image analysis approach for national scale accounting," *ISPRS J. Photogrammetry Remote Sens.*, vol. 175, pp. 1–19, 2021.

[52] L. Yan and D. Roy, "Automated crop field extraction from multi-temporal web enabled landsat data," *Remote Sens. Environ.*, vol. 144, pp. 42–64, 2014.

[53] B. Watkins and A. Van Niekerk, "A comparison of object-based image analysis approaches for field boundary delineation using multi-temporal Sentinel-2 imagery," *Comput. Electron. Agriculture*, vol. 158, pp. 294–302, 2019.

[54] E. Guirado, S. Tabik, D. Alcaraz-Segura, J. Cabello, and F. Herrera, "Deep-learning versus OBIA for scattered shrub detection with Google earth imagery: Ziziphus Lotus as case study," *Remote Sens.*, vol. 9, no. 12, 2017, Art. no. 1220.

[55] H. Huang, Y. Lan, A. Yang, Y. Zhang, S. Wen, and J. Deng, "Deep learning versus object-based image analysis (OBIA) in weed mapping of UAV imagery," *Int. J. Remote Sens.*, vol. 41, no. 9, pp. 3446–3479, 2020.

[56] T. Liu, A. Abd-Elrahman, J. Morton, and V. L. Wilhelm, "Comparing fully convolutional networks, random forest, support vector machine, and patch-based deep convolutional neural networks for object-based wetland mapping using images from small unmanned aircraft system," *GIScience Remote Sens.*, vol. 55, no. 2, pp. 243–264, 2018.

[57] J. Tang, D. Arvor, T. Corpetti, and P. Tang, "Mapping center pivot irrigation systems in the southern Amazon from Sentinel-2 images," *Water*, vol. 13, no. 3, 2021, Art. no. 298.

[58] M. Saraiva, É. Protas, M. Salgado, and C. Souza, "Automatic mapping of center pivot irrigation systems from satellite images using deep learning," *Remote Sens.*, vol. 12, no. 3, 2020, Art. no. 558.

[59] L. Graf, H. Bach, and D. Tiede, "Semantic segmentation of Sentinel-2 imagery for mapping irrigation center pivots," *Remote Sens.*, vol. 12, no. 23, 2020, Art. no. 3937.

[60] Y. Li, H. Qi, J. Dai, X. Ji, and Y. Wei, "Fully convolutional instance-aware semantic segmentation," in *Proc. IEEE Conf. Comput. Vis. Pattern Recognit.*, 2017, pp. 2359–2367.

[61] K. He, G. Gkioxari, P. Dollár, and R. Girshick, "Mask r-CNN," *IEEE Trans. Pattern Anal. Mach. Intell.*, vol. 42, no. 2, pp. 386–397, Feb. 2020.

[62] A. O. de Albuquerque *et al.*, "Instance segmentation of center pivot irrigation systems using multi-temporal Sentinel-1 SAR images," *Remote Sens. Appl.: Soc. Environ.*, vol. 23, 2021, Art. no. 100537.

[63] S. N. de Oliveira, O. A. de Carvalho Jr., R. A. T. Gomes, R. F. Guimaraes, and C. M. McManus, "Landscape-fragmentation change due to recent agricultural expansion in the Brazilian Savanna, Western Bahia, Brazil," *Regional Environ. Change*, vol. 17, no. 2, pp. 411–423, 2017.

[64] S. N. de Oliveira, O. A. de Carvalho Jr., R. A. T. Gomes, R. F. Guimaraes, and C. M. McManus, "Deforestation analysis in protected areas and scenario simulation for structural corridors in the agricultural frontier of Western Bahia, Brazil," *Land Use Policy*, vol. 61, pp. 40–52, 2017.

[65] R. Pousa, M. H. Costa, F. M. Pimenta, V. C. Fontes, V. F. A. d. Brito, and M. Castro, "Climate change and intense irrigation growth in Western Bahia, Brazil: The urgent need for hydroclimatic monitoring," *Water*, vol. 11, no. 5, 2019, Art. no. 933.

[66] M. Drusch *et al.*, "Sentinel-2: ESA's optical high-resolution mission for GMES operational services," *Remote Sens. Environ.*, vol. 120, pp. 25–36, 2012.

[67] T.-Y. Lin *et al.*, "Microsoft COCO: Common objects in context," *Proc. Eur. Conf. Comput. Vis.*, 2014, pp. 740–755.

[68] Y. Wu, A. Kirillov, F. Massa, W.-Y. Lo, and R. Girshick, "Detectron 2," 2019. [Online]. Available: https://github.com/facebookresearch/detectron2

[69] S. Xie, R. Girshick, P. Dollár, Z. Tu, and K. He, "Aggregated residual transformations for deep neural networks," in *Proc. IEEE Conf. Comput. Vis. Pattern Recognit.*, 2017, pp. 1492–1500.

[70] D. Bolya, C. Zhou, F. Xiao, and Y. J. Lee, "YOLACT: Real-time instance segmentation," in *Proc. IEEE/CVF Int. Conf. Comput. Vis.*, 2019, pp. 9157–9166.

[71] D. Bolya, C. Zhou, F. Xiao, and Y. J. Lee, "YOLACT++: Better real-time instance segmentation," *IEEE Trans. Pattern Anal. Mach. Intell.*, p. 1, 2020, doi: 10.1109/TPAMI.2020.3014297.

[72] Z. Cai and N. Vasconcelos, "Cascade r-CNN: Delving into high quality object detection," in *Proc. IEEE Conf. Comput. Vis. Pattern Recognit.*, 2018, pp. 6154–6162.
[73] H. Su *et al.*, "HQ-ISNET: High-quality instance segmentation for remote sensing imagery," *Remote Sens.*, vol. 12, no. 6, 2020, Art. no. 989.
[74] L. Zhong, L. Hu, and H. Zhou, "Deep learning based multi-temporal crop classification," *Remote Sens. Environ.*, vol. 221, pp. 430–443, 2019.
[75] H. Crisóstomo de Castro Filho *et al.*, "Rice crop detection using LSTM, Bi-LSTM, and machine learning models from Sentinel-1 time series," *Remote Sens.*, vol. 12, no. 16, 2020, Art. no. 2655.

Pablo P. de Bem (Member, IEEE) received the B.Sc. degree in forest engineering and the M.Sc. degree in geography in 2014 and 2018, respectively, from the University of Brasília, Brasília, Brazil, where he is currently working toward the Ph.D. degree in geography.

His research interests include applications of remote sensing and GIS in environmental management and forest ecology and machine learning techniques within remote sensing for processes such as land cover classification and change detection.

Anesmar Olino de Albuquerque (Member, IEEE) received the B.Sc. degree in geography from the State University of Goiás, Goiás, Brazil, in 2009 and the M.Sc. degree in geography in 2015 from the University of Brasília, Brasília, Brazil, where he is currently working toward the Ph.D. degree in geography.

He is currently a Researcher with the Laboratory of Space Information and Systems, University of Brasilia.


Roberto Arnaldo Trancoso Gomes (Member, IEEE) received the B.Sc., M.Sc., and Ph.D. degrees in geography from the Federal University of Rio de Janeiro, Rio de Janeiro, Brazil, in 1999, 2002, and 2006, respectively.

He is currently an Associate Professor with the Geography Department, University of Brasília, Brasília, Brazil, where he is also a Professor of the Graduate Program in Geography. His research interests include geosciences and geomorphology, mapping, process modeling, digital image processing, and artificial intelligence.

Dr. Gomes is the Editor of *Revista Espaço & Geografia* and a Reviewer of several scientific journals.
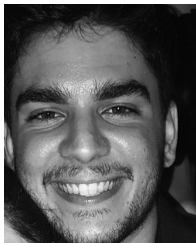
Osmar Luiz Ferreira de Carvalho (Member, IEEE) received the B.Sc. degree in electrical engineering in 2020 from the University of Brasilia, where he is currently working toward the M.Sc. degree in computer science.

He is currently a Machine Learning Engineer in the industry and research projects.

Mr. Carvalho was a Founding Member of the IEEE Computer Intelligence Society Student Chapter, University of Brasilia and was the recipient of the Outstanding Chapter of the Year Award in 2019.

Renato Fontes Guimarães (Member, IEEE) received the B.Sc. degree in cartography engineering from Universidade do Estado do Rio de Janeiro, Rio de Janeiro, Brazil, in 1987, the M.Sc. degree in geophysics from the Observatório Nacional, Rio de Janeiro, Brazil, in 1991, and the Ph.D. degree in geology from the Universidade Federal do Rio de Janeiro, Rio de Janeiro, Brazil, in 2000.

He is currently a Professor with the University of Brasília, Brasília, Brazil. His research interests include geoscience, remote sensing, geomorphology, mathematical modeling, and geoprocessing.

Cristiano Rosa e Silva received the B.Sc. degree in computer science from the Centro Universitário de Anápolis, Anápolis, Brazil, in 2008.

He is currently the CEO of Dubbox Tech, Brasília, Brazil, and works in projects involving artificial intelligence and mobile apps. His research experience involves projects with the Laboratório de Sistemas de Informações Espaciais (LSIE), where he develops software for remote sensing problems.

Osmar Abílio de Carvalho Júnior (Member, IEEE) received the B.Sc., M.Sc., and Ph.D. degrees in geology from the University of Brasília, Brasília, Brazil, in 1990, 1995, and 2000, respectively.

He is currently an Associate Professor with the University of Brasília with broad experience in scientific projects. His research interests include remote sensing, GIS, software development, computer vision, and image classification.

Argelica Saiaka Luiz received the B.Sc. degree in geography from the State University of Goiás, Goiás, Brazil, in 2009 and the M.Sc. degree in geography in 2015 from the University of Brasília, Brasília, Brazil, where she is currently working toward the Ph.D. degree in geography.

She is currently a Researcher with the Laboratory of Space Information and Systems, University of Brasilia.